American Journal of Pathology, Vol. 158, No. 6, June 2001

A Distinctive Pediatric Renal Neoplasm Characterized by Epithelioid Morphology, Basement Membrane Production, Focal HMB45 Immunoreactivity, and t(6;11)(p21.1;q12) Chromosome Translocation

Pedram Argani,* Anita Hawkins,*
Constance A. Griffin,* Jeffrey D. Goldstein,†
Mark Haas,* J. Bruce Beckwith,‡
Carl B. Mankinen,§ and Elizabeth J. Perlman*

From the Department of Pathology, The Johns Hopkins Hospital, Baltimore, Maryland; the Wolfson Children's Hospital,† Jacksonville, Florida; Loma Linda University,‡ Loma Linda, California; and the Cytogenetics Laboratory,§ the Nemours Children's Clinic, Jacksonville, Florida*

We report two cases of a hitherto undescribed pediatric renal neoplasm that is distinctive at the morphological, immunohistochemical, ultrastructural, and cytogenetic levels. On light microscopy, the tumors are composed of nests of polygonal, clear to eosinophilic cells associated with a subpopulation of smaller cells that surround hyaline material. Despite their epithelioid morphology, these tumors do not label immunohistochemically for epithelial markers but instead label focally for melanocytic markers HMB45 and Melan A. The hyaline material is positive with periodic acid-Schiff and methenamine-silver histochemical stains, and labels immunohistochemically for type 4 collagen. Ultrastructural examination confirms that it represents basement membrane material. Cytogenetic analysis reveals the identical t(6;11)(p21.1;q12) chromosome translocation as the sole abnormality in these two tumors, confirming their identity and distinctive nature. ***(Am J Pathol 2001, 158:2089–2096)***

The classification of pediatric renal neoplasms that are composed of nonembryonal, epithelioid cells is fraught with difficulty. The major diagnostic considerations are carcinoma and epithelioid angiomyolipoma (AML). Renal cell carcinomas (RCCs) of the type seen in adults are well known to arise within the pediatric kidney, particularly clear cell carcinomas in the setting of von Hippel-Lindau syndrome and papillary RCCs.[1] In addition, there are at least two distinctive variants of renal carcinoma that preferentially affect young patients. One of these is a cytogenetically distinct variant characterized by a t(X;1)(p11.2;q21) chromosome translocation,[2] although the morphological spectrum of this molecularly defined entity has not been systematically studied. Another is the recently defined renal medullary carcinoma, a high-grade and highly lethal tumor that preferentially affects patients with sickle cell trait.[3] The pure epithelioid variant of AML, also known as renal epithelioid oxyphilic neoplasm, consists entirely of nests of polygonal oncocytic cells with well-defined cell borders.[4,5] As it lacks the other features typically seen in AML (fat, dysplastic arterioles) and frequently demonstrates cytological atypia in the form of tumor giant cells, this lesion is easily mistaken for RCC. In fact, many of the tumors previously classified as RCC in children with the tuberous sclerosis syndrome have proved to be epithelioid AML.[6–8] Most of these lesions stain intensely for the melanocytic marker HMB45 but not for epithelial markers.[9] The existence of epithelioid neoplasms other than RCCs and renal epithelioid oxyphilic neoplasm in the pediatric kidney is not well established, although experience suggests that not all lesions fit into the above categories.

We report two cases of a hitherto undescribed pediatric renal neoplasm that is distinctive at the microscopic, immunohistochemical, ultrastructural, and genetic levels. Although their morphological features suggest that they represent an epithelial neoplasm, these tumors are nonimmunoreactive for epithelial markers. Like AMLs, they are focally immunoreactive for melanocytic markers; however, their ultrastructural features are distinct from both RCC and AML. On cytogenetic analysis, these tumors bear the identical t(6;11)(p21.1;q12) chromosome translocation, supporting the concept that they represent a distinctive morphological and molecular entity.

Accepted for publication February 16, 2001.

Address reprint requests to Pedram Argani, M.D., The Johns Hopkins Hospital, Surgical Pathology, 2242 Weinberg Building, 401 N. Broadway, Baltimore, MD 21231-2410. E-mail: pargani@pds.path.jhu.edu.

Materials and Methods

Case 1 was encountered in the routine surgical pathology signout at The Johns Hopkins Hospital. Case 2 was subsequently encountered in the consultation files of JBB. Tissue from each case was fixed in 10% neutral-buffered formalin and routinely processed for light microscopy.

For immunohistochemical labeling, four-μm sections were deparaffinized with xylene for 30 minutes and rehydrated using graded ethanol concentrations. Antigen retrieval was performed using either protease digestion or steaming. Immunoperoxidase labeling using the avidin-biotin-peroxidase complex technique and 3′,3′-diaminobenzidine as chromagen was performed with the automated Biotek-1000 staining system (Ventana/Biotek Solutions, Inc., Tucson, AZ). The antibodies used, vendors, pretreatments, and dilutions were as follows: epithelial membrane antigen (EMA) (steam, 1:1000; DAKO, Carpinteria, CA), desmin (steam, 1:20,000; DAKO), S100 protein (steam, 1:6000; DAKO), smooth muscle actin (steam, 1:200; Boehringer Mannheim, Indianapolis, IN), cytokeratin 7 (protease, 1:50; DAKO), vimentin (steam, 1:100; Zymed, San Francisco, CA), cytokeratin AE1/AE3 (protease, 1:2000; Boehringer Mannheim), cytokeratin Cam5.2 (protease, prediluted; Becton Dickinson, San Jose, CA), HMB45 (steam, 1:125; DAKO), and Melan A (steam, 1:800; DAKO). To avoid biotin-related staining artifacts, labelings for HMB45, Melan-A, Cam 5.2, and cytokeratin 7 were repeated using the DAKO Envision system instead of the avidin-biotin-peroxidase technique.

For ultrastructural analysis, fresh samples of tumor were fixed in 3% glutaraldehyde and then postfixed in 1% osmium tetroxide, followed by dehydration and embedding in epoxy resin. Ultrathin sections stained with lead citrate and uranyl acetate were examined in a Philips CM12 transmission electron microscope.

For cytogenetic analysis, tumor tissue from each patient was prepared by mincing and digestion with collagenase type II, then cultured for 2 to 4 days. Cells were harvested after 1 to 5 hours exposure to colcemid at 0.6 μg/ml, slides were made and G-banded after standard protocols. Twenty cells were analyzed from tumor 1 and six mitotic figures were analyzed from tumor 2. Chromosome abnormalities were described according to the 1995 International System for Human Cytogenetic Nomenclature guidelines. An additional slide for tumor 1 was made for spectral karyotyping (SKY) analysis according to the protocol supplied with the probe kit (Applied Spectral Imaging, Carlsbad, CA). The SKY probe was a mixture of whole chromosome paint probes for each chromosome, combinatorially labeled with five fluorochromes. Briefly, the probe was denatured, pre-annealed with Cot-1 DNA for 1 hour, hybridized with the separately denatured chromosomes for 48 hours, washed, and detected according to ASI (Carlsbad, CA) protocol. Eleven metaphases were analyzed for hybridization quality, and four representative cells were chosen for complete analysis. Metaphase images were acquired using a standard epifluorescence microscope equipped with a 150 W xenon lamp, a 63× oil-immersion objective, and the ASI SpectraCube SD200 system. 4′,6-Diamidino-2-phenylindole-counterstained images were captured with a 100 W mercury lamp and inverted by Sky View software (ASI) to permit enhanced banding.

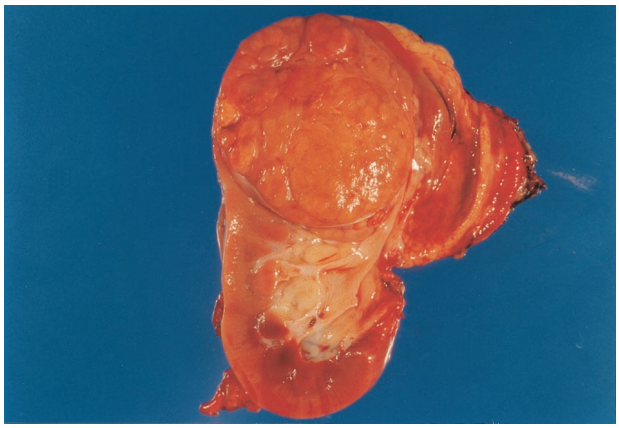

Figure 1. Gross photograph of tumor 1. The tumor is well-delineated, nodular, and brown. Smaller yellow nodules lie within.

Results

Case Histories

Patient 1 was an 18-year-old African-American male with a past medical history significant only for asthma who presented with gross hematuria associated with left flank pain after traumatic injury. Abdominal ultrasonography and computed tomography scan demonstrated a 7-cm left renal mass. The patient underwent an uncomplicated left radical nephrectomy. He is known to be alive 18 months after surgery, although the status of his tumor is not known. He has not received postoperative chemotherapy or radiation therapy.

Patient 2 was a 10-year-old African-American male with a past medical history significant for precocious puberty associated with elevated serum somatomedin C levels. He developed painless hematuria, and was found to have a right renal mass. The patient underwent an uncomplicated right radical nephrectomy. He has not received postoperative chemotherapy or radiation therapy. The patient is alive and free of tumor by renal ultrasonography and chest X-ray 26 months after surgery. Computed tomography scan performed 12 months after surgery similarly showed no evidence of tumor.

In neither case was a history of von Hippel-Lindau syndrome or of tuberous sclerosis syndrome elicited.

Gross Findings

Patient 1's tumor was located in the upper pole of the left kidney, and measured 7 × 7 × 6.5 cm. On cut section, the tumor was well circumscribed, tan-brown in color, and had a multinodular appearance. Slightly more yellow

Figure 2. Low-power view of tumor 2, showing nested pattern and infiltration among native renal elements at the tumor's leading edge (H&E; original magnification, ×100).

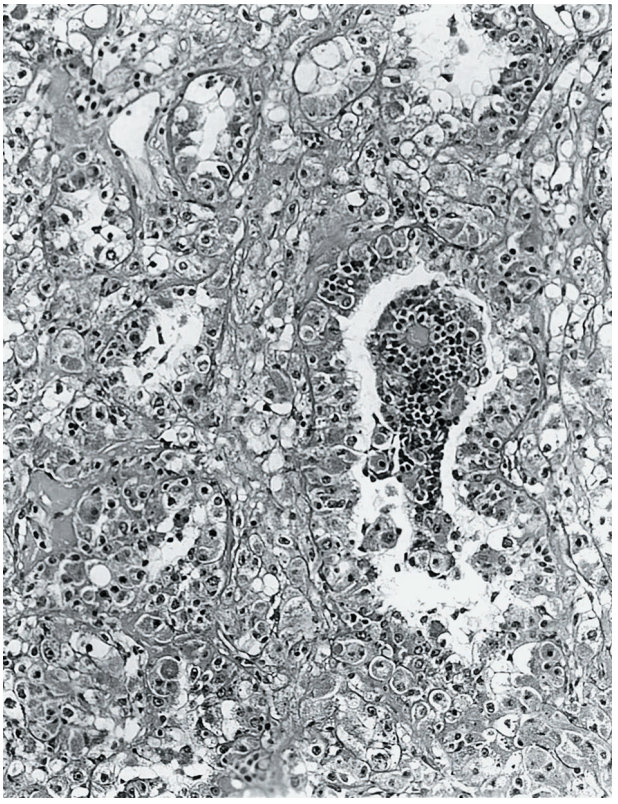

Figure 3. Low-power view of tumor 1, showing acinar pattern of growth with clusters of smaller cells surrounding basement membrane material located within an acinus (H&E; original magnification, ×100).

nodules could be appreciated within (Figure 1). Neither necrosis nor hemorrhage was identified. The tumor was confined by the renal capsule, but extended into the renal pelvis. Patient 2's tumor replaced nearly the entire anterior and central kidney, with normal kidney discernable only in the medial upper and lower poles. The tumor measured 12.2 × 9.7 × 7.1 cm, and on cut section it too was primarily tan-brown and nodular, with other more golden yellow areas. Small blood-filled cysts measuring up to 3.4 cm were also identified, but necrosis was not seen. This tumor also was confined to the kidney.

Microscopic Findings

The two tumors were distinctive and virtually identical at the microscopic level, and therefore they are described together. Each tumor was surrounded in part by a thin, focally calcified, fibrous capsule. However, each tumor permeated this capsule multifocally to infiltrate superficially among native renal tubules. The tumors were predominantly composed of nests of polygonal cells with well-defined cell borders, separated by thin capillaries (Figure 2). Occasional staghorn-shaped, thin-walled vessels were also present. The capillaries became inapparent in more cellular, solid areas of the tumor. In other areas, the tumor demonstrated an acinar growth pattern (Figure 3). The polygonal tumor cells had variable cytoplasmic morphology: some cells had completely clear cytoplasm, others had pale, sparsely granular, pink cytoplasm, whereas others had densely granular, eosinophilic cytoplasm (Figure 4). Nuclei were generally rounded, although at high power one could appreciate the slightly irregular nuclear contours and small central nucleoli. Also scattered throughout these tumors were 10 to 50 cell clusters of smaller cells that characteristically surrounded small rounded nodules of hyaline, basement membrane-like material, yielding an appearance reminiscent of Call-Exner bodies. These clusters often appeared to be present within acini formed by the larger, polygonal cells (Figure 3), and were particularly prominent in cytological smear preparations made from case 1 (Figure 5). Overall, the variably clear to eosinophilic cytoplasm of the polygonal cells and the scattering of smaller cells gave these tumors a polymorphous appearance (Figure 4). The hyaline material was positive on periodic acid-Schiff stain, both before and after diastase treatment, and on methenamine silver stain, consistent with basement membrane material (not shown).

Neither tumor demonstrated appreciable mitotic activity or necrosis microscopically. Each subtly penetrated into intrarenal and renal sinus vasculature, the latter finding making them stage 2 using National Wilms Tumor Study-5 criteria. Tumor 1 extended into the renal pelvis to undermine renal pelvic urothelium, whereas tumor 2 compressed the renal medulla, causing congestion. Neither tumor extended beyond the renal capsule microscopically. Abnormalities of the nonneoplastic kidney, such as nephrogenic rests or dysplasia, were not identified.

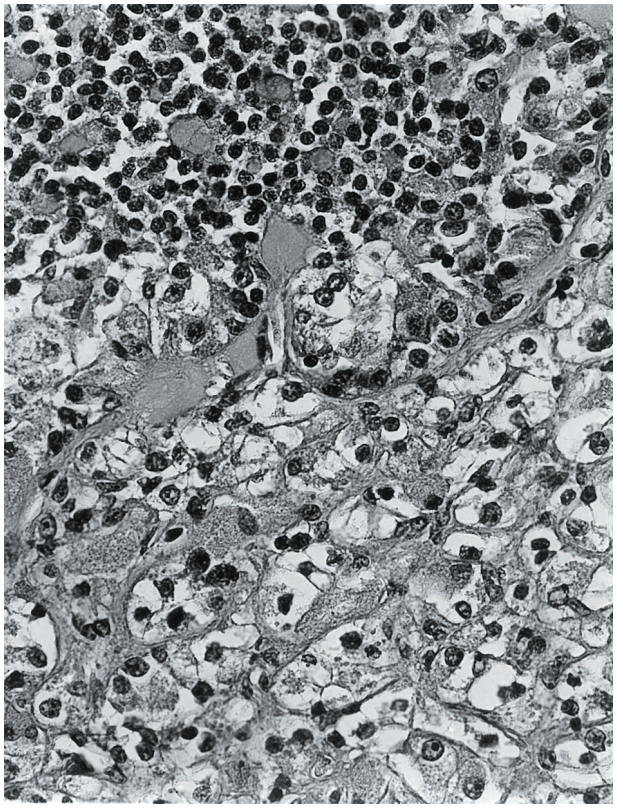

Figure 4. High-power view of tumor 2, showing larger epithelioid cells with fine granular cytoplasm adjacent to smaller cells that are associated with basement membrane material (H&E; original magnification, ×400).

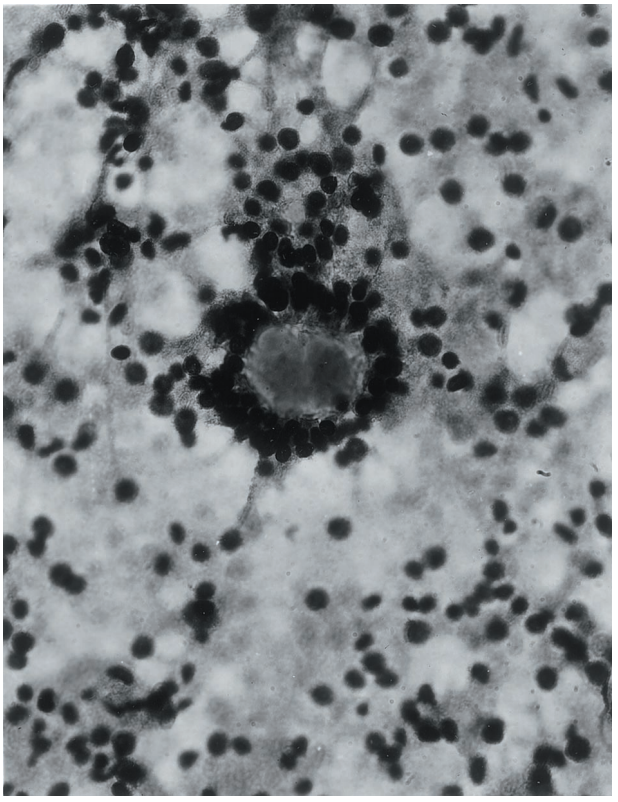

Figure 5. Smear preparation of tumor 1, showing smaller cells clustered around basement membrane material (H&E; original magnification, ×400).

Immunohistochemical Findings

Each tumor, particularly the more eosinophilic cells, was immunoreactive for vimentin. The tumors were nonimmunoreactive for a wide range of epithelial markers including cytokeratin AE1/AE3, cytokeratin Cam 5.2, cytokeratin 7, and EMA. The epithelial markers highlighted the infiltrative border of these tumors, as scattered, intensely keratin-positive entrapped renal tubules were identified at the tumor's leading edge (Figure 6). A moderate number of epithelioid tumor cells labeled focally but intensely for the melanocytic markers HMB45 and Melan-A, although these stains were not diffusely positive and did not label the smaller cells (Figure 7). Stains for S100 protein, desmin, smooth muscle actin, and chromogranin A did not label the tumor cells. The pink hyaline material about which the smaller cells were clustered labeled strongly for type 4 collagen. This marker also highlighted the tumor's prominent capillary vasculature (Figure 8).

Ultrastructural Findings

Electron microscopic examination revealed polygonal cells with abundant mitochondria and scattered membrane-bound granules, some also containing prominent amounts of glycogen. The most prominent feature was the presence of localized pools of duplicated basement membrane material surrounded by clusters of tumor cells (Figure 9, A and B). The larger nests of tumor cells were also

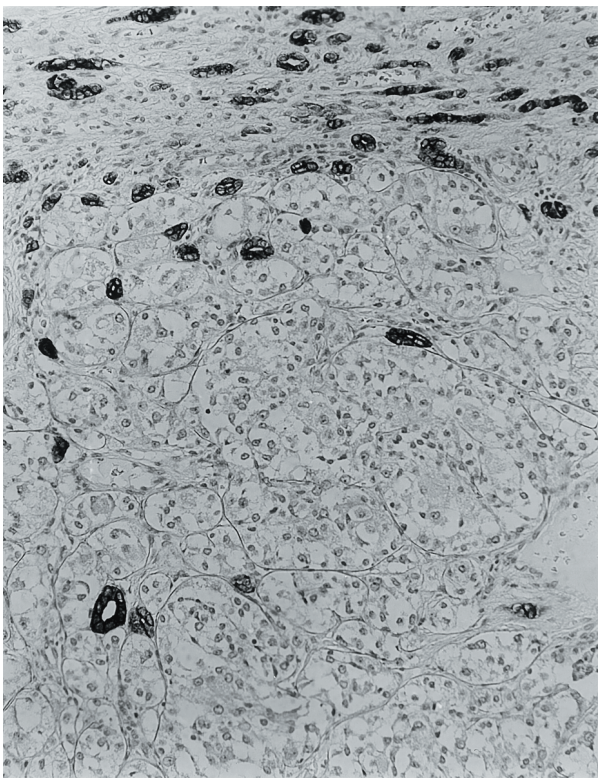

Figure 6. Immunohistochemical stain for cytokeratin AE1/3 demonstrates cytokeratin-negative tumor infiltrating among cytokeratin-positive native renal tubules (avidin-biotin-peroxidase; original magnification, ×160).

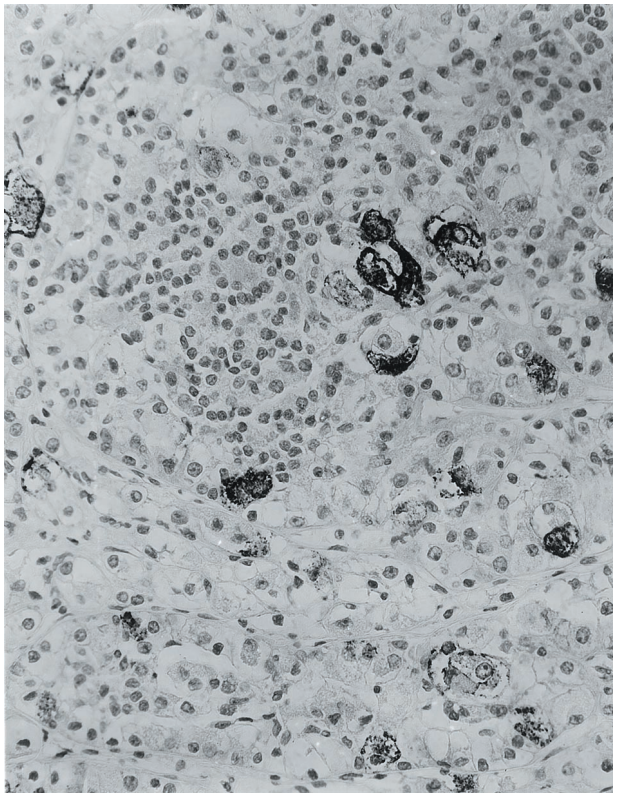

Figure 7. Immunohistochemical stain for HMB45 demonstrates scattered intensely positive epithelioid cells in a background of predominantly negative epithelioid cells and smaller cells (DAKO Envision labeling; original magnification, ×250).

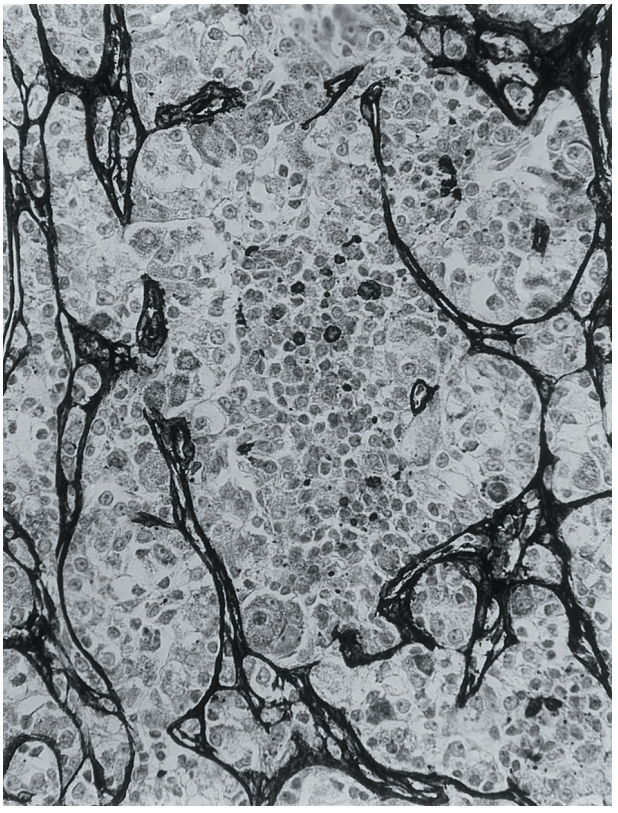

Figure 8. Immunohistochemical stain for type 4 collagen highlights the nested quality of the tumor vasculature and labels the hyaline material between the smaller cells, indicating that it is basement membrane (avidin-biotin peroxidase; original magnification, ×250).

delineated by basement membrane. Occasional cell junctions were identified (Figure 9B), but true desmosomes were not. Cytoplasmic filaments were not prominent.

Cytogenetic Findings

All G-banded cells from both patient's tumors contained a balanced translocation between chromosomes 6 and 11 as the sole abnormality. Although the translocation for patient 1 was initially interpreted as a whole-arm translocation, t(6;11)(p10;p10) (Figure 10), SKY analysis showed the translocation breakpoints to be clearly within the short arm of chromosome 6 and the long arm of chromosome 11 (Figure 11). The breakpoint in the der(11) seems to be within 11q12 or at the 11q12-q13 junction; however, we cannot exclude the possibility that the breakpoint occurs in the light material of the very proximal 11q13.1. The description of the karyotype was corrected to 46, XY, t(6;11)(p21.1;q12) for both patients.

Discussion

We report two renal neoplasms of childhood which are distinctive at the morphological, immunohistochemical, ultrastructural, and cytogenetic levels. These tumors feature nests of epithelioid, polygonal cells that suggest the diagnosis of carcinoma at the light microscopic level. However, unlike carcinomas, the tumor cells do not label immunohistochemically for epithelial markers and do not demonstrate desmosomes at the ultrastructural level. Like epithelioid AML, the tumors label for melanocytic markers HMB45 and Melan A; however, labeling is only focal in these tumors whereas it is typically diffuse in epithelioid AML. Furthermore, unlike most AML, the cells do not contain the distinctive, pleomorphic membrane-bound granules that resemble premelanosomes at the ultrastructural level.[5] Instead, the cells produce distinctive aggregates of basement membrane material, evident microscopically as pink hyaline globules. The tumors each bore the identical t(6;11)(p21.1;q12) chromosome translocation, confirming their distinctive nature.

The histogenesis of these tumors is not clear, as their ultrastructural features do not match those of any normal cell within the kidney. Production of duplicated basement membrane material is a characteristic of two neoplasms, adenoid cystic carcinoma and cylindroma, which are far different from these lesions at the morphological and immunophenotypic levels and not well-recognized to occur within the kidney.[10] It remains possible that these tumors are related to epithelioid AML, as is suggested by their morphology and reactivity for melanocytic markers. Epithelioid AML is one of a family of lesions thought to be derived from perivascular epithelioid cells (PECs).[11] These cells are found in many of the hamartomatous lesions associated with tuberous sclerosis syndrome, such as AML, cardiac rhabdomyoma, and pulmonary

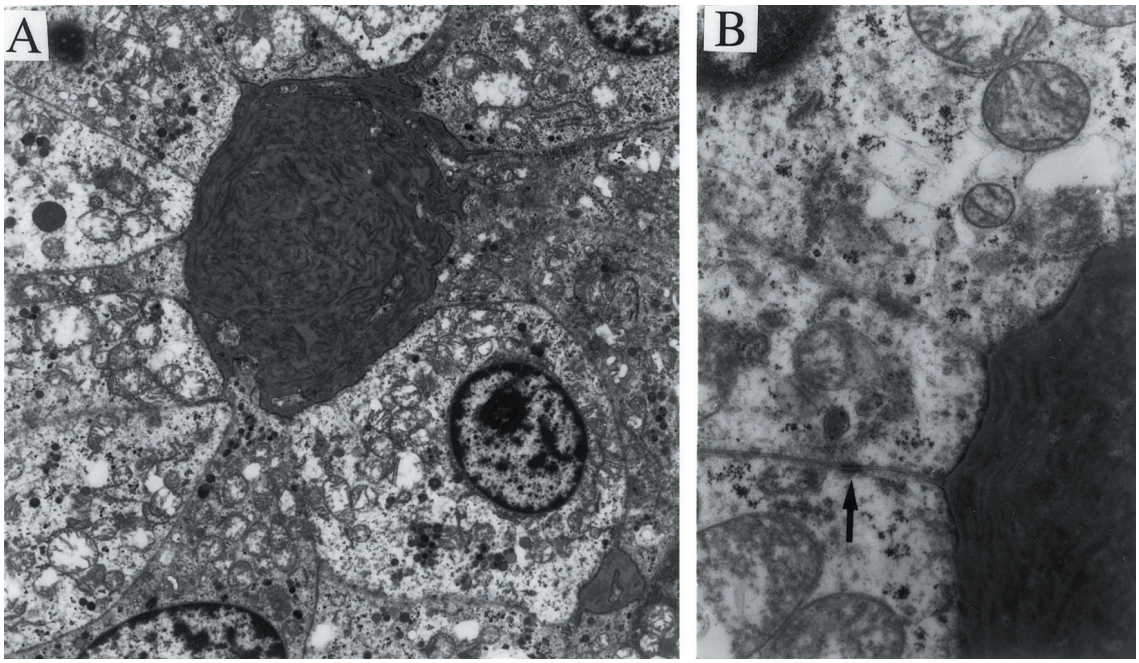

Figure 9. Electron microscopy of tumor from patient 1. **A:** Low-power electron micrograph shows tumor cells surrounding a pool of basement membrane material. The cytoplasm of the tumor cells contains prominent mitochondria, scattered membrane-bound granules, and varying amounts of glycogen (uranyl acetate and lead citrate stain; original magnification, ×3000). **B:** Higher power micrograph shows the multilamellar appearance of the basement membrane material, and an intercellular junction (**arrow**) (uranyl acetate and lead citrate stain; original magnification, ×13,000).

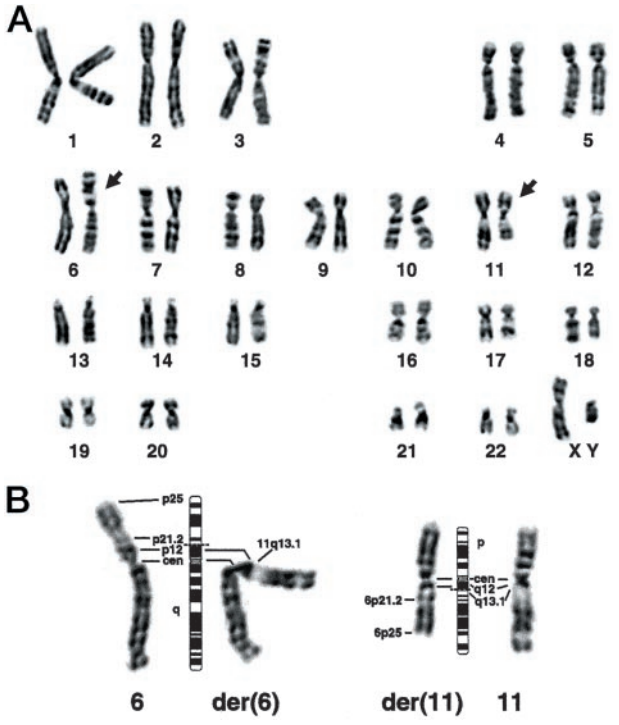

Figure 10. A: Representative 46, XY, t(6;11)(p21.1;q12) G-banded karyotype for patient 1; **arrows** indicate the rearranged chromosomes. Although the breakpoints seem to be at the centromere yielding a whole arm translocation, the chromosomes are placed in the karyotype as defined by the SKY results (Figure 11). **B:** Partial karyotype showing the normal and derivative chromosomes from another cell, with their respective 550-band idiograms. **Dashed lines** indicate the presumptive breakpoints.

lymphangioleiomyomatosis.[12] PECs classically co-express myogenic and melanocytic markers; however, they are thought to be capable of dramatically modulating their morphology and immunophenotype. For example, spindled PECs express muscle markers like actin more strongly than HMB45, whereas the converse is true of

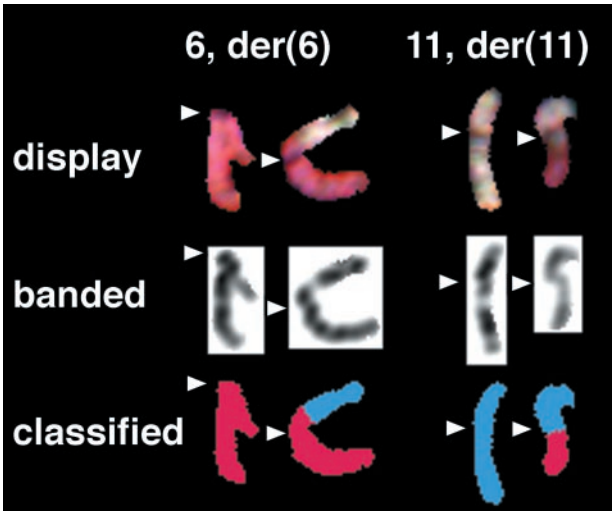

Figure 11. Partial karyotypes after SKY hybridization; **arrowheads** indicate the centromere position, showing that the breakpoints are in the short arm of chromosome 6 and the long arm of chromosome 11. In the display image (**top**), the repetitive sequences near the centromere cause a gap in the paint probe signal where unlabeled Cot reduces hybridization. The color is clearly seen to continue on the opposite side of the centromere of both derivative chromosomes. The centromere may also be seen as a constriction in the inverted 4′,6-Diamidino-2-phenylindole-banded image of the same chromosome (**center**). Automatic classification of the hybridized chromosomes by the SKY system (**bottom**) confirms that the chromosome 6 material extends into the p-arm of the der(6), and the chromosome 11 material extends into the q-arm of the der(11).

epithelioid PECs. Because occasional epithelioid AML have been found to express cytokeratins[6,13] and have been associated with overt RCC,[14,15] some have also postulated that PECs can modulate into a fully epithelial phenotype.[16,17] Modulation of PECs toward adipocytic differentiation can explain predominantly adipocytic AML and microhamartomas of the kidney. Perhaps the current lesions represent another phenotype toward which the PECs can modulate, one which is characterized by abundant basement membrane production and only focal HMB45 immunoreactivity. In favor of this theory is the fact that PECs of AML are normally associated with basement membrane material, although it is usually discontinuous. It is intriguing that focal intense HMB45 immunoreactivity similar to that which we observed in these tumors has been reported in two other lesions, the leiomyoma of the renal capsule[18] and cardiac rhabdomyoma.[12] The latter is associated with the tuberous sclerosis syndrome.

Although the t(6;11)(p21.1;q12) chromosome translocation has not previously been reported, it is of interest that loci near each breakpoint involved in the translocation have been implicated in renal disease. Translocations involving 11q13 are implicated in a subset of renal oncocytomas;[19,20] the reciprocal partners for these translocations have most frequently been located on the long arm of chromosome 9[21,22] and the long arm of chromosome 5 (specifically 5q35).[23,24] 11q13 is known to harbor mitochondrial genes, and disruption of this locus is postulated to effect the mitochondria-rich phenotype of oncocytoma. Along these lines, it is intriguing that the current lesions demonstrate prominent mitochondria at the ultrastructural level, although not to the degree of oncocytoma. However, the published karyotypes from oncocytoma seem to show a breakpoint in distal 11q13, and a published fluorescence *in situ* hybridization study[24] places it within 11q13.3. Our tumors show a breakpoint barely past the centromere, in 11q12 or very proximal 11q13.1, and thus rearrangement at the same locus seems unlikely. The 6p21 locus has been implicated in multicystic renal dysplasia, in one case via a t(6;19)(p21;q13.1) translocation that disrupts the *CDC5L* gene.[25,26] Neither of the loci implicated in tuberous sclerosis (*TSC1* at 9q34 or *TSC2* at 16p13.3) are involved in the t(6;11)(p21.1;q12) translocation. However, deletion of 11q13 was identified in 2 of 11 AMLs studied by comparative genomic hybridization, including one epithelioid variant.[27]

In summary, we present two cases of a distinct tumor type characterized by epithelioid cell morphology, immunoreactivity for melanocytic markers, prominent basement membrane material ultrastructurally, and a unique t(6;11)(p21.1;q12) chromosome translocation. These tumors seem to be rare, although we have subsequently encountered several morphologically and immunohistochemically similar lesions from which material for cytogenetic analysis was unavailable. Although both of our cases were identified in young patients, it is possible that this reflects the bias inherent in our clinical practice. These cases illustrate the challenges that pediatric renal tumors can pose at the morphological level, and the value of cytogenetics in defining distinctive entities.

Acknowledgments

We thank Manju Kaushal and Selva Murugesan for assistance with the immunohistochemical staining.

References

1. Renshaw AA, Granter SR, Fletcher JA, Kozakewich HP, Corless CL, Perez-Atayde AR: Renal cell carcinomas in children and young adults: increased incidence of papillary architecture and unique subtypes. Am J Surg Pathol 1999, 23:795–802
2. Meloni AM, Dobbs RM, Pontes JE, Sandberg AA: Translocation (X;1) in papillary renal carcinoma: a new cytogenetic subtype. Cancer Genet Cytogenet 1993, 65:1–6
3. Davis Jr CJ, Mostofi FK, Sesterhenn IA: Renal medullary carcinoma: the seventh sickle cell nephropathy. Am J Surg Pathol 1995, 19:1–11
4. Martigoni G, Pea M, Bonetti F, Zamboni G, Carbonara C, Longa L, Zancanaro C, Maran M, Brisigotti M, Mariuzzi GM: Carcinoma-like monotypic epithelioid angiomyolipoma in patients without evidence of tuberous sclerosis: a clinicopathologic and genetic study. Am J Surg Pathol 1998, 22:663–672
5. Eble JN, Amin MB, Young RH: Epithelioid angiomyolipoma of the kidney: a report of five cases with a prominent and diagnostically confusing epithelioid smooth muscle component. Am J Surg Pathol 1997, 21:1123–1130
6. Bjornsson J, Short MP, Kwiatkowski DJ, Henske EP: Tuberous-sclerosis-associated renal cell carcinoma: clinical, pathologic, and genetic features. Am J Pathol 1996, 149:1201–1208
7. Pea M, Bonetti F, Martignoni G, Henske EP, Manfrin E, Cloato C, Bernstein J: Apparent renal cell carcinomas in tuberous sclerosis are heterogeneous: the identification of malignant epithelioid angiomyolipoma. Am J Surg Pathol 1998, 22:180–187
8. Al-Saleem T, Wessner LL, Scheithauer BW, Patterson K, Roach ES, Dreyer SJ, Fujikawa K, Bjornsson J, Bernstein J, Henske EP: Malignant tumors of the kidney, brain, and soft tissue in children and young adults with the tuberous sclerosis complex. Cancer 1998, 83:2208–2216
9. Bacchi CE, Bonetti F, Pea M, Martignoni G, Gown AM: HMB-45. A review. Appl Immunohistochem 1996, 4:73–85
10. Erlandson RA: Diagnostic Electron Microscopy of Tumors. New York, Raven Press, 1994, pp 249–252, 274–276, 740–742
11. Bonetti F, Pea M, Martigoni G, Zamboni G, Manfrin E, Colombari R, Mariuzzi GM: The perivascular epithelioid cell and related lesions. Adv Anat Pathol 1997, 4:343–358
12. Weeks DA, Chase DR, Malott RL, Chase RL, Zuppan CW, Beckwith JB, Mierau GW: HMB-45 staining in angiomyolipoma, cardiac rhabdomyoma, other mesenchymal processes, and tuberous-sclerosis associated brain lesions. Int J Surg Pathol 1994, 1:191–198
13. Martignoni G, Pea M, Rigaud G, Manfrin E, Colato C, Zamboni G, Scarpa A, Tardanico R, Roncalli M, Bonetti F: Renal angiomyolipoma with epithelioid sarcomatous transformation and metastasis. Am J Surg Pathol 2000, 24:889–894
14. Csansky G, Szereday Z, Magyarlaki T, Mehes G, Herbert T, Buzogany I: Renal angiomyolipoma: report of three cases with regional lymph node involvement and/or with renal cell carcinoma. Tumori 1995, 81:469–474
15. Rosai J: Ackerman's Surgical Pathology, ed 8. St. Louis, Mosby, 1996, pp 1156–1157
16. Mai KT, Perkins DG: Letter to the editor. Am J Surg Pathol 1999, 23:356–357
17. Mai KT, Perkins DG, Collins JP: Reply to letter to the editor. Histopathology 1996, 29:491–493
18. Bonsib SM: HMB-45 immunoreactivity in renal leiomyomas and leiomyosarcomas. Mod Pathol 1996, 9:664–669
19. Neuhaus C, Dijkhuizen T, van den Berg E, Storkel S, Stockle M, Mensch B, Huber C, Decker H-J: Involvement of the chromosomal region 11q13 in renal oncocytoma: case report and literature review. Cancer Genet Cytogenet 1997, 94:95–98
20. Fuzesi L, Gunawan B, Braun S, Bergmann F, Brauers A, Effert P, Mittermayer C: Cytogenetic analysis of 11 renal oncocytomas: further evidence of structural rearrangements of 11q13 as a characteristic chromosomal abnormality. Cancer Genet Cytogenet 1998, 107:1–6

21. Fuzesi L, Gunawan B, Braun S, Boeckmann W: Renal oncocytoma with a translocation t(9;11)(p23;q13). J Urol 1994, 152:471–472
22. Walter TA, Pennington RD, Decker H-JH, Sandberg AA: Translocation t(9;11)(p25;q12): a primary chromosomal change in renal oncocytoma. J Urol 1989, 142:117–119
23. Van den Berg E, Dijkhuizen T, Storkel S, de la Riviere GB, Dam A, Mensink HJA, Oosterhuis JW, de Jong B: Chromosomal changes in renal oncocytomas. Evidence that t(5;11)(q35;q13) may characterize a second subgroup of oncocytomas. Cancer Genet Cytogenet 1995, 79:164–168
24. Sinke RJ, Dijkhuizen T, Janssen B, Weghuis DO, Merkx G, van den Berg E, Schuuring E, Meloni AM, de Jong B, van Kessel AG: Fine mapping of the renal oncocytoma-associated translocation (5;11)(q35;q13) breakpoint. Cancer Genet Cytogenet 1997, 96:95–101
25. Groenen PM, Vanderlinden G, Devriendt K, Fryns JP, Van de Ven WJ: Rearrangements of the human CDC5L gene by a t(6;19)(p21;q13.1) in a patient with multicystic renal dysplasia. Genomics 1998, 49:218–229
26. Robson WLM, Rogers RC, Leung AKC: MCDK, UPJO, and VUR: a common genetic cause. Am J Med Genet 1995, 59:396–398
27. Kattar MM, Grignon DJ, Eble JN, Hurley PM, Lewis PE, Sakr WE, Cher ML: Chromosome analysis of renal angiomyolipoma by comparative genomic hybridization: evidence for clonal origin. Hum Pathol 1999, 30:295–299